A High-Accuracy Multiwavelength Radiometer for In Situ Measurements in the Thermal Infrared. Part I: Characterization of the Instrument

MICHEL LEGRAND, CHRISTOPHE PIETRAS,* GÉRARD BROGNIEZ, AND MARTIAL HAEFFELIN+

Laboratoire d'Optique Atmosphérique, Université des Sciences et Technologies de Lille, Villeneuve d'Ascq, France

NADER KHALIL ABUHASSAN* AND MICHAËL SICARD

CIMEL Electronique, Paris, France

(Manuscript received 1 October 1998, in final form 25 October 1999)

ABSTRACT

The new infrared radiometer (conveyable low-noise infrared radiometer for measurements of atmosphere and ground surface targets, or CLIMAT) is a highly sensitive field instrument designed to measure brightness temperatures or radiances in the infrared, from the ground level, or from an aircraft. It can be equipped with up to six channels in the 8–14-μm range. This instrument is characterized by its portability (total mass less than 5 kg), its self-sufficiency, and its automated operation. It can be operated either manually or automatically. The optical head of the instrument contains an objective lens and a condenser mounted according to the Köhler design, providing a uniform irradiation on the detector and a well-delimited field of view. The radiation is measured by a low-noise fast thermopile whose responsivity is slightly temperature dependent. The radiometric noise expressed as an equivalent brightness temperature is on the order of 50 mK for a 1-μm bandwidth at room temperature. The application of a thermal shock reveals no noticeable degradation of the measurements, even though the cavity of the thermopile is not stabilized in temperature.

1. Introduction

Many satellites equipped with infrared radiometers measuring the radiation emitted by the earth–atmosphere system were launched in the past three decades. According to a simplified description, they can be classified into three categories. Some of them are instrumented to achieve the specific task of measuring the radiative budget of the earth–atmosphere system, such as ERBE (Earth Radiation Budget Experiment; Barkstrom and Smith 1986), CERES (Cloud and Earth Radiant Energy System; Wielicki et al. 1996), and ScaRaB (Scanner Radiatsionnogo Balansa) on board *Meteor-3/7* (Kandel et al. 1998). For meteorological purposes, the World Weather Watch was implemented by the WMO (World Meteorological Organization) in 1968. Weather observation is performed thanks to a ring of geostationary satellites including Meteosat (Europe) (Mason and Schmetz 1992), GOES-East and GOES-West (United States), GMS (Japan), INSAT (India), GOMS (Russia), and FY-2 (China); associated to sun-synchronous NOAA (National Oceans and Atmosphere Administration) platforms equipped with AVHRR (Advanced Very High Resolution Radiometer) instruments. The third category includes many satellites devoted to various remote sensing applications relevant to the earth surface and its atmosphere, such as Landsat/TM (Thematic Mapper), ATSR (Along Track Scanning Radiometer) on board the ERS (European Remote Sensing Satellite) satellite (Mutlow et al. 1994), and OCTS (Ocean Color and Temperature Scanner) onboard the Japanese satellite ADEOS (Advanced Earth Observing System) (Igarashi 1997).

The spaceborne radiometers in operation generally have several channels in the thermal infrared spectral domain. They are characterized by a high radiometric precision. New sensors to be developed in the next ten years will still be improved (Chédin and Scott 1991; King et al. 1992; Phulpin and Chevrel 1994; Durpaire et al. 1995).

To face this development, it appears necessary to have accurate multichannel infrared radiometers available to operate in ground-based as well as in airborne modes,

* Current affiliation: GSC–NASA Goddard Space Flight Center, Greenbelt, Maryland.

+ Current affiliation: Virginia Tech/NASA LaRC, Hampton, Virginia.

Corresponding author address: Dr. Michel Legrand, Laboratoire d'Optique Atmosphérique, Université des Sciences et Tech. de Lille, Villeneuve d'Ascq Cedex 59655, France.
E-mail: michel.legrand@univ-lille1.fr

for calibration, validation, and analysis of data acquired by spaceborne instruments.

So far, some laboratories have developed accurate radiometers for their own use (e.g., see Platt 1971; Hepplewhite 1989). Concurrently, commercial models are available to the scientific community. Among the most known, are models from the Barnes Engineering Company (currently manufactured by Pyrometer Instrument Company, Inc., Northvale, New Jersey). These instruments have often been considered as standards, and they have been widely used over the past 30 years, either ground-based or on board aircrafts, for measuring radiances and brightness temperatures in the 8–14-μm spectral region (e.g., Saunders 1967, 1970; Lorenz 1968; Weiss 1971; Fouquart et al. 1987; Saunders and Minnett 1990; Brogniez et al. 1995). The principle of these single-channel instruments of the former generation involves a chopping mirror mounted in front of an optical system. A bolometer detector is placed at the focus of the optics. The delivered signal is processed through a synchronous detection.

As things stand, we considered the available instruments inadequate with regard to the need of satellite applications. So, we deemed it worthwhile to develop a new radiometer, adapted to the characteristics of the current and forthcoming spaceborne instruments, as well as to the specific constraints of ground-based and airborne operations, and which could take advantage of the technological progress of the last decades. The project of developing and qualifying such an instrument was jointly decided in 1992 by scientists from four French institutes, namely, the Institut National de la Recherche Agronomique, Monfavet; the Groupement Scientifique de Télédétection Spatiale, Strasbourg; the Centre de Recherches Géophysiques du CNRS, Garchy; the Laboratoire d'Optique Atmosphérique (LOA), Université de Lille.

This project was implemented in 1993 and 1994 (Abuhassan 1995; Pietras 1996), in collaboration with the manufacturer CIMEL Electronique, Paris, France.

The multichannel radiometer (conveyable low-noise infrared radiometer for measurements of atmosphere and ground surface targets, or CLIMAT) is the result of this collaboration. It uses a thermopile as sensor. Its output voltage and cold junction temperature are measured and used to derive the radiance and brightness temperature of a viewed target. Instead of a chopper, it includes a retractable mirror used at will.

Section 2 describes the instrument principle and its main characteristics. We present the performances of the prototype studied at the LOA in section 3. The instrument performances for in situ operations are analyzed in a companion paper (Part II of this paper).

2. Description of the instrument

CLIMAT is designed to perform measurements in the thermal infrared domain. It is primarily designed for ground-based observations but is also suited for operation on board an aircraft or from any vehicle. This radiometer is made up of an optical head and a control unit. With an overall mass less than 5 kg, it is remarkably light. It is powered by internal batteries, which can be charged by panels of solar cells, or by the mains via an AC/DC converter. Figure 1 shows a picture of the prototype of the instrument CLIMAT.

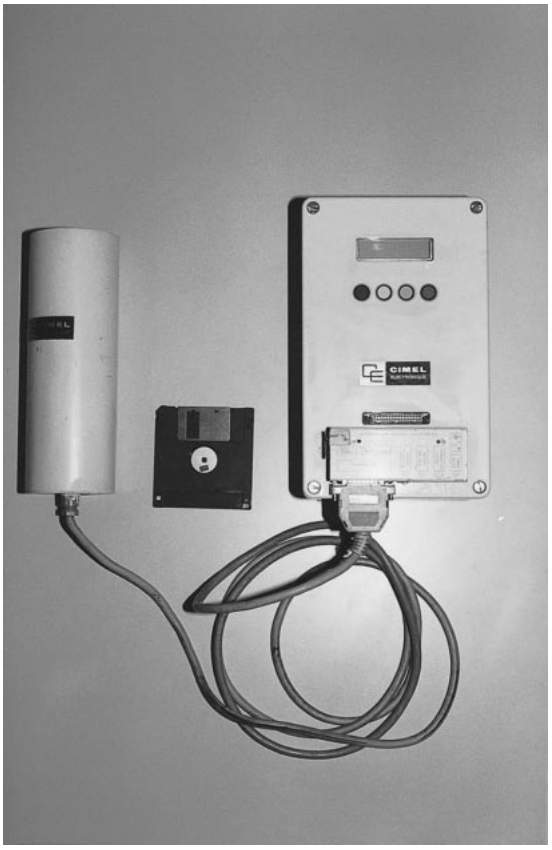

FIG. 1. The prototype of the radiometer CLIMAT. Left: optical head. Right: electronic unit. The scale is indicated by a 3.5″ floppy disk.

a. Optical design

The block diagram of the optical head is shown in Fig. 2. The objective (O) is a standard convex-plane germanium lens, and the condenser (C) is a ''best-shaped'' germanium meniscus designed to minimize the geometrical aberrations. The main characteristics of these lens are shown in Table 1. They are treated on both sides with a nonreflective coating. The condenser is located in the focal plane of the objective. The detector (D), equipped with a germanium window (W), is positioned in the conjugate plane of the objective, with respect to the condenser. This so-called Köhler design (Jamieson et al. 1963) has the following advantages.

- The radiance from a remote target is uniformly dis-

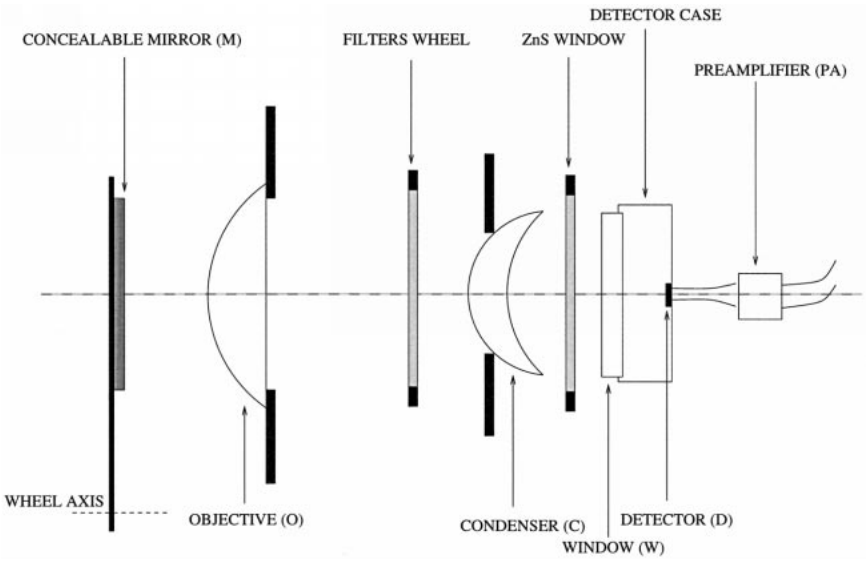

FIG. 2. Synoptic scheme of the optical head.

tributed on the objective; so the detector, located in the conjugate plane, is also uniformly illuminated, avoiding hot spots and preventing biases due to the nonuniform sensitivity of its surface.

- The theoretical field of view (FOV) is defined through the ratio of the diameter of the condenser to its distance to the objective. All the rays coming from the target delimited by the theoretical FOV, and incident to the objective, reach the detector. On the contrary, no ray coming from outside this FOV can reach the detector. So the real FOV is geometrically well defined, coinciding with the theoretical one, and the instrument produces negligible vignetting.
- The possibility exists of changing the FOV, just by replacing the objective by a lens with a different focal length, making the instrument versatile.

The cavity containing the detector is used as a reference of temperature and radiation. Its temperature is accurately monitored by a platinum probe. A retractable gold-plated mirror (M), located in front of the optical head, allows the radiations originating from the target and from the thermopile cavity to be compared, whenever necessary. The mirror is set on a wheel controlled with a stepper motor driven by a microprocessor. Its reflection coefficient, as given by the manufacturer, reaches a value of 99.74%.

A filters wheel located between the lenses can have up to six interference filters. A second stepper motor is used to select the desired filter. The prototype of CLIMAT is equipped with only three interference filters (see section 2b).

TABLE 1. Lens characteristics of the optical head of the prototype CLIMAT.

	Focal length (mm)	Effective diameter (mm)
Objective	25.40	5.60
Condenser	3.23	4.35

For wavelengths greater than 15 μm, the incident radiation is blocked by a zinc sulfide filter located between the condenser and the detector.

Optimal positions of the different components of the instrument optics and a best value for the diameter of the entrance diaphragm were determined using a Monte Carlo ray-trace model. This first-principle instrument model was initially developed to characterize the optical and radiative performance of spaceborne broadband radiometers (Haeffelin et al. 1997). The ray-trace code was adapted to accurately represent the CLIMAT radiometer geometry and optical components in order to assist experimental studies of the instrument through its development phase.

b. Optical components

1) LENSES AND DETECTOR WINDOW

The spectral transmittances of the condenser, objective, and detector window are provided by the manufacturers between 8 and 14 μm. We checked the spectral transmittance of the objective with a spectrometer, but were not able to do so with the other two components due to their small diameter. However, their transmittances at 10.6 μ m for a normal incidence were measured using a CO_2 laser. The results are shown in Table 2.

2) INTERFERENCE FILTERS AND ZNS WINDOW

The filters wheel of the prototype is equipped with three narrowband interference filters labeled N9 (8.2–

TABLE 2. Transmittance of the optical components measured for a normal incidence using a CO_2 laser at 10.6 μm.

Objective	Condenser	Detector window
0.98	0.98	0.87

9.2 μm), N11 (10.5–11.5 μm), and N12 (11.5–12.5 μm). A fourth broadband channel labeled W (8–14 μm) can be selected using a position of the wheel without filter. The spectral transmittances of these filters and of the ZnS window were carefully measured using three different spectrometers. The values were found to be in close agreement and an average of the measured transmittance was derived for each filter. The overall spectral transmittance of every channel is obtained by making the product of the measured spectral transmittances of the optical components placed on the path of the measured radiation. The spectral transmittance functions are shown in Fig. 3 for the four channels of the prototype. To explain the choice of the spectral band pass of the instrument channels, the transmittance of the *U.S. Standard* Atmosphere (McClatchey et al. 1971) is shown in Fig. 3 along a vertical path, for the 8–14-μm atmospheric window.

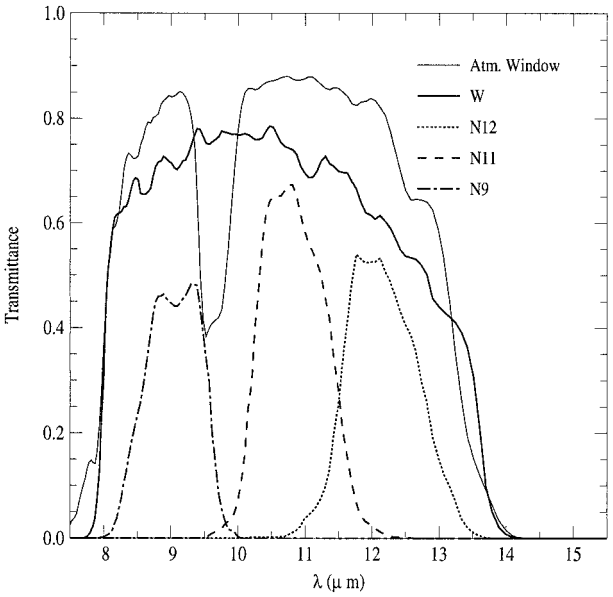

FIG. 3. Spectral transmittance of the four channels of the prototype CLIMAT. The transmittance of the *U.S. Standard* Atmosphere is added for comparison purpose.

c. Detector

Quantum detectors are faster and more sensitive than thermal detectors. However, they need to be cooled down in order to be efficient in the longwave range, which makes them difficult to use as field instruments. In addition, their detectivity is spectrally dependent and vanishes above a given wavelength threshold. Thermal detectors, however, can be operated at room temperature and their detectivity is independent of the wavelength. Hence, we selected a thermopile as detector for our instrument. The output voltage of a thermopile varies proportionally to the temperature difference between its cold and hot junctions. The model 1M manufactured by Dexter (Dexter Research Center, Inc., Dexter, Michigan), was selected. Its main characteristics are shown in Table 3. The hot junction is heated by the incident radiation, while the cold junction is at the temperature of the thermopile substrate, which is also the ambient temperature of the cavity. The temperature dependence of the thermopile responsivity is weak.

From an electrical point of view, the thermopile is a low-pass filter, adapted to a low chopping frequency, or no chopping. The radiometer CLIMAT has no chopping system. Instead, the reference radiation can be measured, by rotating the mirror wheel, either repeatedly for each target measurement, or at specific times—for instance, when the temperature of the cavity varies significantly. The signal-to-noise ratio of the detector increases as the dwell of an individual measurement increases. The measurements are usually 1 s long (i.e., corresponding to a unit bandwidth of frequency). The noise equivalent power (NEP) is given in Table 3, precisely for a unit bandwidth of frequency. However, the measurements can be done faster. The detector time constant (see Table 3) allows a minimum dwell time of about 20 ms, suitable for airborne applications.

d. Electronics

The electronics is entirely made up of conductive metal oxide semiconductor (CMOS) components, resulting in a low electrical consumption. It is reliably protected by tight boxes. The electronics of the optical head and of the control unit are described hereafter.

1) INTERNAL ELECTRONICS OF THE OPTICAL HEAD

A synoptic scheme of the electronics in the optical head is presented in Fig. 4. The output voltage of the

TABLE 3. Characteristics of the thermopile at the temperature of 296 K. (Model 1M from Dexter Research Center, Inc.)

Active area	(0.6×0.6) mm^2
Number of junctions	40
Resistor	60 kΩ
Voltage noise	31.3 nV Hz$^{-1/2}$
Responsivity	120 V W^{-1}
Responsivity temperature coefficient α	-0.15% K^{-1}
Noise equivalent power (NEP)	0.26 nW Hz$^{-1/2}$
D^*	2.3×10^8 cm W^{-1} Hz$^{-1/2}$
Time constant	12 ms
Field of view	80°
Germanium window with nonreflective coating	8–14 μm

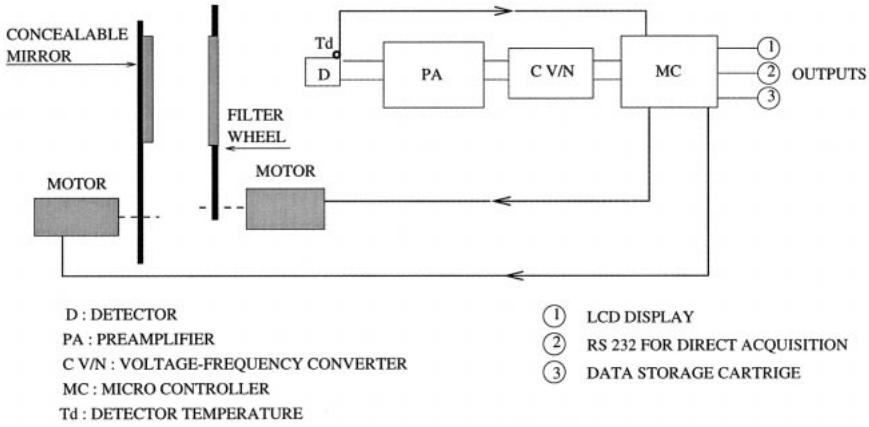

FIG. 4. Synoptic scheme of the electronics.

detector ranges between ±3 mV depending on the radiances from the target and in the cavity temperature. The amplification line consists of a low-noise preamplifier (PA) with a gain of 1000, a voltage–frequency converter (C V/N) with a conversion factor of 10^4 Hz V^{-1}, and a microcontroller (MC), which acts as a pulse counter.

2) CONTROL UNIT ELECTRONICS

The electronics of the control unit includes a microprocessor, which controls the measurements and operates the stepper motors for the mirror motion and the filters commutation. An internal memory of 32 kbytes allows a storage capacity of several hours of continuous measurements. Cartridges are available for external data storage, each of them allowing an autonomy of several days (depending on the frequency of data acquisition). Data recovery and external management of the radiometer through a personal computer (PC) is possible via a serial port. The control unit can manage an external robot used to direct the optical head in any zenithal and azimuthal viewing directions.

A keyboard associated to a liquid crystal screen allows measurements and various informations stored in the memory to be displayed, such as digitized output signal, date and hour, detector temperature, batteries voltage, and filters in use. It also allows the instrument operating mode, either the PC-driven mode or the automated internal mode, to be selected.

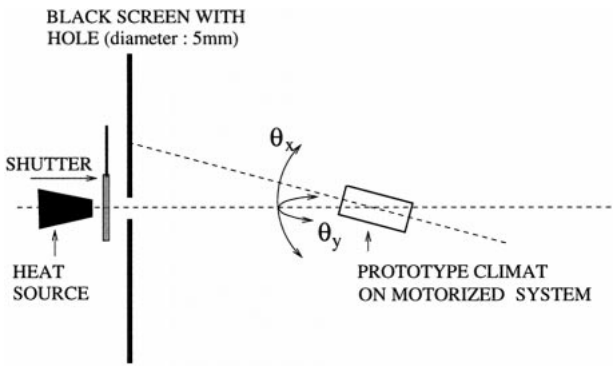

FIG. 5. Experimental setup for the determination of the field of view.

3. Performances

a. Field of view

Taking advantage of the Köhler design, the prototype FOV (≃10°), is expected to be geometrically well-defined. An experiment was carried out in order to accurately describe this FOV. A schematic of the experimental setup is presented in Fig. 5. A circular aperture 5-mm diameter is drilled through a black screen, and a hot pinpoint source (realized by means of a soldering iron) is located immediately behind it. The radiometer is located about 1 m away from this radiant source characterized by a very small area compared to the footprint of the FOV on the screen (≃0.08%).

A shutter is introduced between the radiant source and the screen in order to remove the background signal from the screen through a differential measurement. For every viewing direction of the optical head, defined according to the two angular coordinates (θ_x, θ_y), a differential measurement is made. The results are presented in Fig. 6. The FOV is well delimited between −5° and +5°. However, we note that the maximum response is not exactly centered on the instrument optical axis. The nonaxisymmetric feature in the instrument response can be due to one or a combination of the following effects: (i) heterogeneity of the thermopile sensor surface related to the arrangement of junctions; (ii) possible nonuniformity of the nonreflective coatings used on some of the lenses and filters, in particular the zinc sulfide filter located between the condenser and detector; (iii) assembly uncertainties in term of location and orientation of some of the instrument components with respect to optical axis. The Monte Carlo ray-trace model, de-

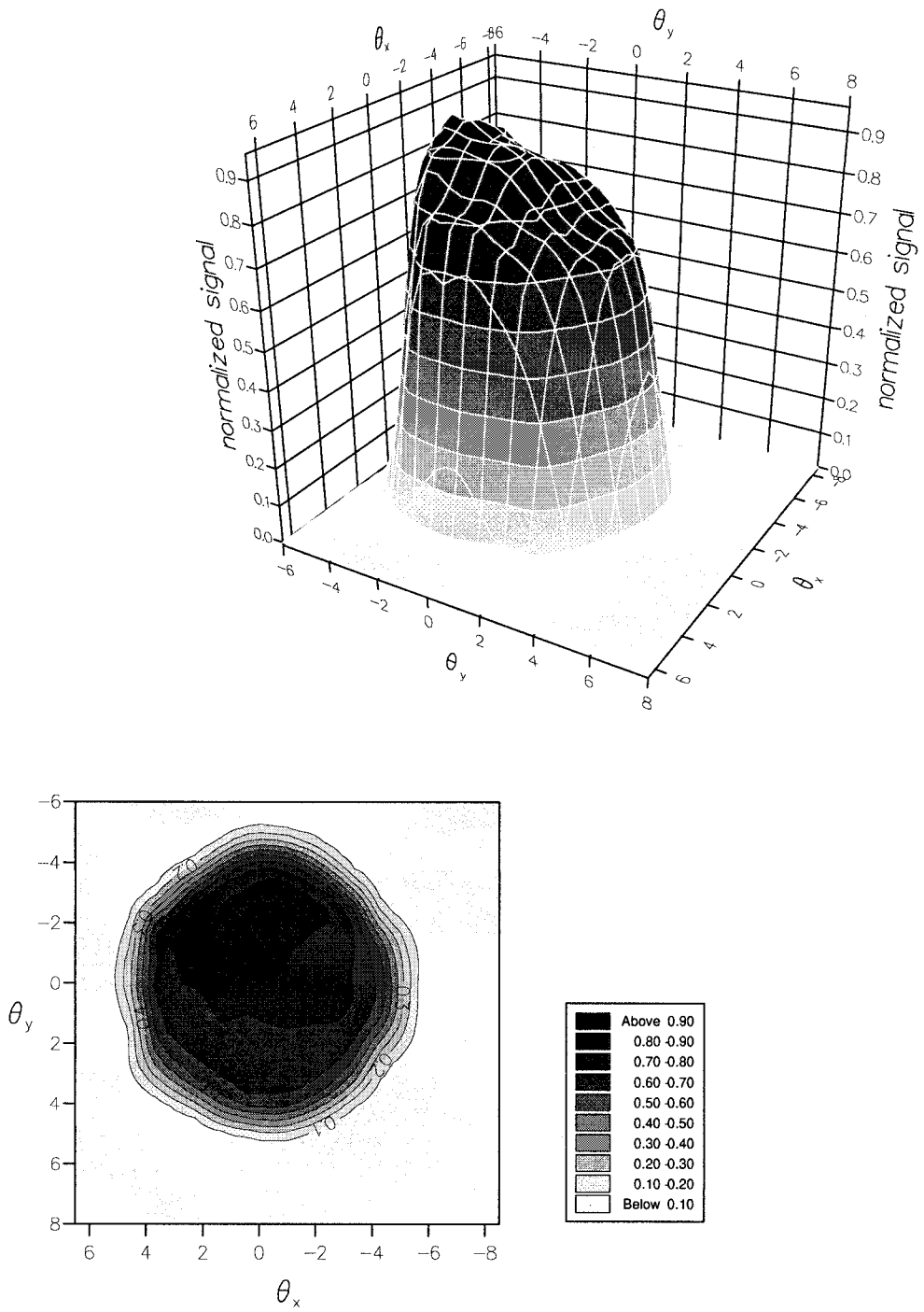

FIG. 6. Measured relative directional response.

scribed in section 2a, is used to determine the sensitivity of the instrument response to assembly uncertainties. Nonuniformity of coatings could also be addressed with the model, but information about the structure of coatings could not be obtained from the manufacturer. Our study is limited to the effects of the location of the detector and the orientation of the condenser on the instrument signal response. Because of the Köhler design, the detector and condenser location and orientation are most critical. The implications related to each component are studied separately. Figure 7 depicts the assembly uncertainty associated with these components. For each assembly default, a one-dimensional density distribution function is determined by computing the

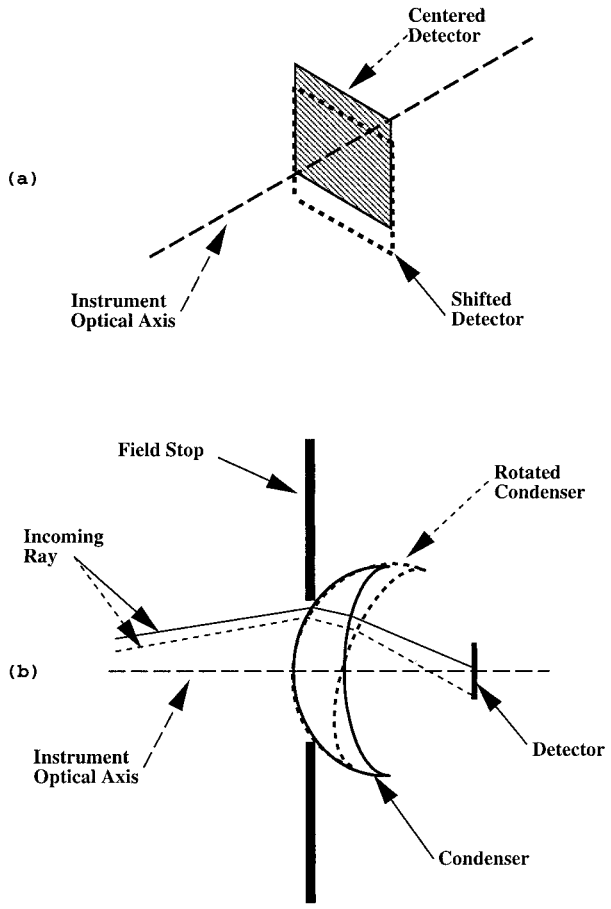

FIG. 7. The geometry of the assembly uncertainties of (a) the detector and (b) the condenser.

response of the instrument to collimated radiation incident to the instrument aperture at different angles. The entire FOV is sampled from $-5°$ to $+5°$ with a 0.5° step size. Figure 8 shows the normalized response of the instrument as a function of the angle of incidence of collimated radiation given the uncertainty on the location of the center of the detector with respect to the optical axis to be about 0.15 mm and the rotation of the condenser on the field stop to about 2.5°. The solid line represents the normalized response for a noncentered detector and the dashed line for a rotated condenser. Both uncertainties lead to very similar asymmetry in the distribution function, with a maximum 100% response for an incidence of about $-2.5°$ off the optical axis and 70% response for a 2.5° incidence. Note that these simulations reproduce quantitatively the experimental results shown in Fig. 6. According to the manufacturing company, CIMEL Electronique, the uncertainty in the assembly procedure of the detector is on the order of 0.05 mm with respect to the optical axis and the rotation of the condenser on the field stop is known to about 1.0°. Given these facts and the results from the Monte Carlo analysis, it is reasonable to conclude that the non-axisymmetry of the instrument response is not only due to assembly uncertainties but also to manufacturing uncertainties of optical and sensing components.

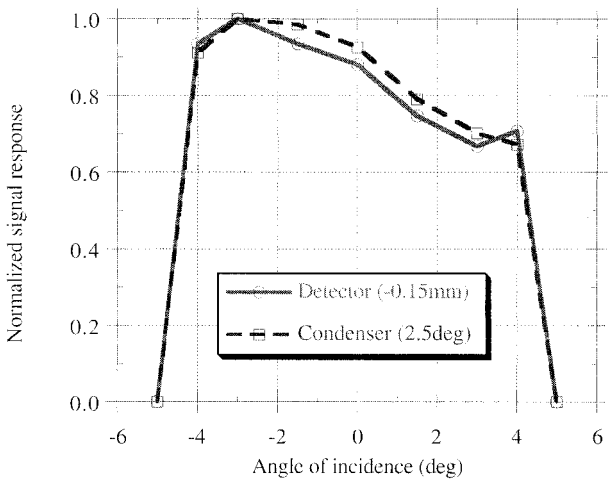

FIG. 8. Simulated normalized response of the CLIMAT radiometer as a function of the angle of incidence of collimated radiation (°) with off-centered detector and condenser.

b. *Calibration and retrieval of brightness temperature*

The radiometric calibration is performed by viewing a blackbody source at a variable temperature T, measured by a calibrated platinum probe. The detector temperature T_d is measured by a second calibrated platinum probe paired with the previous one. The outgoing radiance $L_i(T)$ from the blackbody source at the temperature T, through channel i of the radiometer, is given by

$$L_i(T) = \int_{\Delta_i\lambda} B_\lambda(T)\tau_i(\lambda)\, d\lambda, \tag{1}$$

where $B_\lambda(T)$ is the Planck's function for a blackbody at temperature T, $\tau_i(\lambda)$ and $\Delta_i\lambda$ are, respectively, the spectral transmittance and the bandwidth of channel i. The radiance $L_i(T)$ is accurately fitted to the temperature T by the empirical equation

$$L_i(T) = a_i \exp\left(-\frac{b_i}{T^{n_i}}\right), \tag{2}$$

which establishes a relationship between radiance and blackbody temperature, simpler than Eq. (1), and easy to invert.

The three parameters a_i, b_i, and n_i of Eq. (2) are given in Table 4, for $L_i(T)$ expressed in mW cm^{-2} sr^{-1} and T in kelvins. The fitting precision on the derived temperature is better than 0.02% for all channels, throughout the entire temperature range (190, 320 K).

The relevant quantity for calibration of channel i is the difference in digital counts Δc_i between the output

TABLE 4. Values of the parameters fitting the radiance, expressed in mW cm^{-2} sr^{-1}, to blackbody temperature, expressed in kelvins, for each channel [see Eq. (2)].

Channel i	W	N12	N11	N9
a_i	770.16	48.63	89.65	128.48
n_i	0.867	0.931	0.949	0.967
b_i	762.15	879.51	1060.00	1373.07

signals delivered by the radiometer viewing successively the blackbody at temperature T and its cavity at temperature T_d.

A fit of $\Delta c_i = c_i(T) - c_i(T_d)$ versus $\Delta L_i = L_i(T) - L_i(T_d)$ is obtained using a linear regression

$$\Delta c_i = S_i \Delta L_i, \tag{3}$$

where S_i is the radiometric sensitivity of channel i, at the detector temperature T_d. Figure 9 shows calibration curves for each of the four channels of the prototype. When sensing a target through channel i with a cavity at temperature T_d, these curves allow the measured radiometric counts to be converted into a radiance difference ΔL_i. The radiance $L_i(T_d)$ is computed, applying Eq. (2), and the target radiance $L_i(T_i)$ is derived from ΔL_i and $L_i(T_d)$. The temperature T_i is the target brightness temperature from channel i, which is computed using the reciprocal of Eq. (2).

However, the cavity is not temperature-stabilized, and when its temperature T'_d is different from the temperature T_d used during calibration, the derivation of the brightness temperature T_i must be modified. Applying Eq. (3), the measured signal becomes

$$\Delta c'_i = S'_i \Delta L'_i, \tag{4}$$

where $\Delta L'_i = L_i(T_i) - L_i(T'_d)$ and $\Delta c'_i = c'_i(T_i) - c'_i(T'_d)$. The sensitivity S'_i in Eq. (4) is slightly different from S_i in Eq. (3) because the thermopile responsivity has a weak temperature dependence. It is expressed as

$$S'_i = S_i \exp(\alpha \Delta T_d), \tag{5}$$

where $\Delta T_d = T'_d - T_d$, and α is the (negative) responsivity temperature coefficient of the detector, specified by the manufacturer (see Table 3).

Finally, from Eqs. (2), (3), and (4), the brightness temperature of the target, in the channel i becomes

$$T_i = \left\{ -\frac{\ln\left[\dfrac{\Delta c'_i}{a_i S'_i} + \exp\left(-\dfrac{b_i}{T'^{n_i}_d}\right)\right]}{b_i} \right\}^{-1/n_i}. \tag{6}$$

c. Long-term stability of the sensitivity

The sensitivity values and the corresponding confidence interval at the 95% significance level resulting

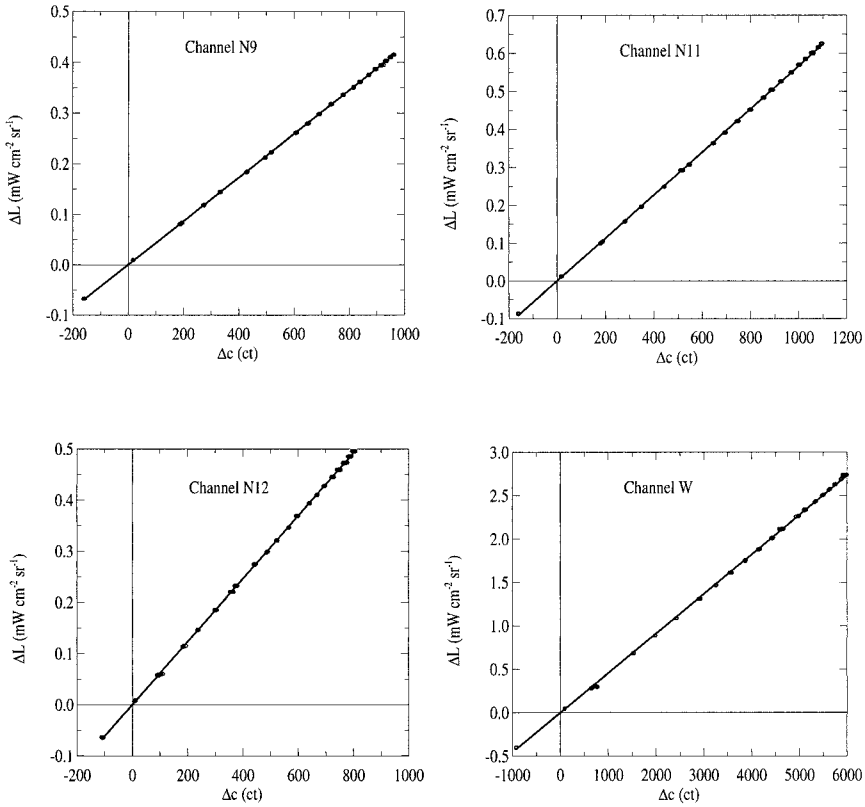

FIG. 9. Radiance calibration of the four channels. The temperature of the detector was T_d = 292.8 K.

TABLE 5. Sensitivity values and their confidence interval significant at the 95% level [in counts (mW cm^{-2} sr^{-1})$^{-1}$] for the successive calibrations of the prototype CLIMAT.

Date	T_d (K)	W	N12	N11	N9
14 Dec 1994	292.5	2212.6 ± 3.4	1624.3 ± 3.6	1743.6 ± 4.6	2325.1 ± 3.8
04 Apr 1995	292.8	2194.1 ± 2.0	1619.7 ± 2.0	1763.8 ± 1.2	2318.4 ± 1.0
27 Jul 1995	299.6	2182.1 ± 1.9	1606.4 ± 2.6	1752.8 ± 1.8	2292.1 ± 1.0

from the successive calibrations of the prototype are given in Table 5 for the four channels. Only small variations of the sensitivity not exceeding 1.4% are observed throughout a period of 7 months, demonstrating the stability of the radiometer over such a period. The improved accuracy obtained on the sensitivity values after the 14 December 1994 stems from some perfecting in the calibration handling.

d. Error analysis

We estimate the absolute uncertainty ΔT_i on the determination of the brightness temperature T_i of a target by using Eq. (6). Three kinds of uncertainties are identified: (i) ΔT_i^c due to the uncertainty in numerical output counts, associated with detector and electronic noise and digitizing of the output voltage; (ii) ΔT_i^p due to the uncertainty in the temperatures given by the platinum probes; and (iii) ΔT_i^s due to the uncertainty in the sensitivity S_i obtained from calibration. As a first approximation, by considering these various sources of uncertainty as independent, we estimate the total uncertainty ΔT_i as

$$\Delta T_i = [(\Delta T_i^c)^2 + (\Delta T_i^p)^2 + (\Delta T_i^s)^2]^{1/2}. \quad (7)$$

1) OUTPUT SIGNAL NOISE

The optical head of the radiometer and a blackbody were placed facing each other in a chamber at 296 K during a long enough time to ensure an accurate thermal equilibrium. The fluctuation measurements of the output signal allowed to determine a standard deviation σ_c of 0.82 counts for 1-s measurements (i.e., for a 1-Hz bandwidth). Converting 0.82 counts into an equivalent detector output voltage gives 82 nV Hz$^{-1/2}$, which includes noise generated by the detector, the electronics, and roundoff errors due to data digitizing. For comparison, the detector noise specified by the manufacturer is 32 nV Hz$^{-1/2}$(Table 3).

For each channel i, it is then possible to derive the noise equivalent power NEP_i (expressed in W), and the noise equivalent difference of temperature NEDT_i (in K), according to (e.g., see Wolfe and Zissis 1989):

$$\mathrm{NEP}_i = \frac{\sigma_c A\Omega}{S_i}, \quad (8)$$

$$\mathrm{NEDT}_i = \frac{\mathrm{NEP}_i}{\dfrac{dL_i}{dT}A\Omega} = \frac{\sigma_c}{S_i\dfrac{dL_i}{dT}} \quad (9)$$

where S_i is the sensitivity defined in Eq. (3), dL_i/dT is the derivative of the radiance of channel i with respect to the blackbody temperature, A is the pupil entrance area, and Ω is the FOV solid angle. Instrument noise parameters values are given in Table 6, for each channel of the prototype, and for two target temperatures.

TABLE 6. Values of various noise parameters measured for a 1 − Hz bandwidth, for each channel of the prototype CLIMAT, with target temperatures of 296 and 223 K, respectively.

Channel i	W	N12	N11	N9
NEP (nW)	1.50	2.10	1.96	1.46
NEDT (mK) (T = 296 K)	7.3	61.7	41.3	41.1
NEDT (mK) (T = 223 K)	19.7	134.5	104.3	137.1

2) PLATINUM PROBE UNCERTAINTIES

The accuracy of each platinum probe once paired is evaluated to be 0.04 K at room temperature, including the roundoff error of digitization.

3) CALIBRATION UNCERTAINTY

The calibration provides values of radiance sensitivity S_i for each channel. Every measured point (output signal and probe temperature) involves a slight scatter, which results in an uncertainty on S_i (Table 5).

4) GLOBAL UNCERTAINTY

These various errors can be summed up using Eq. (7) to estimate a total uncertainty ΔT_i on the retrieved target brightness temperature T_i. The results are summarized in Fig. 10 for each channel of the instrument. These values assess the overall absolute error on brightness temperature measurements (noises plus biases). Noise on the differential output data Δc_i is estimated from ΔT_i^c alone.

Long-term sensitivity shifts as given in Table 5 also obviously induce additional biases. Considering the extreme values of sensitivity obtained for each channel, over the period of seven months, separating the first calibration from the third one, provides error drifts ΔT_i^d summarized in Table 7. It is interesting to compare these errors to the accuracy performances presented in Fig. 10. Their presence would substantially increase the overall error on the measurements. So, it is advisable

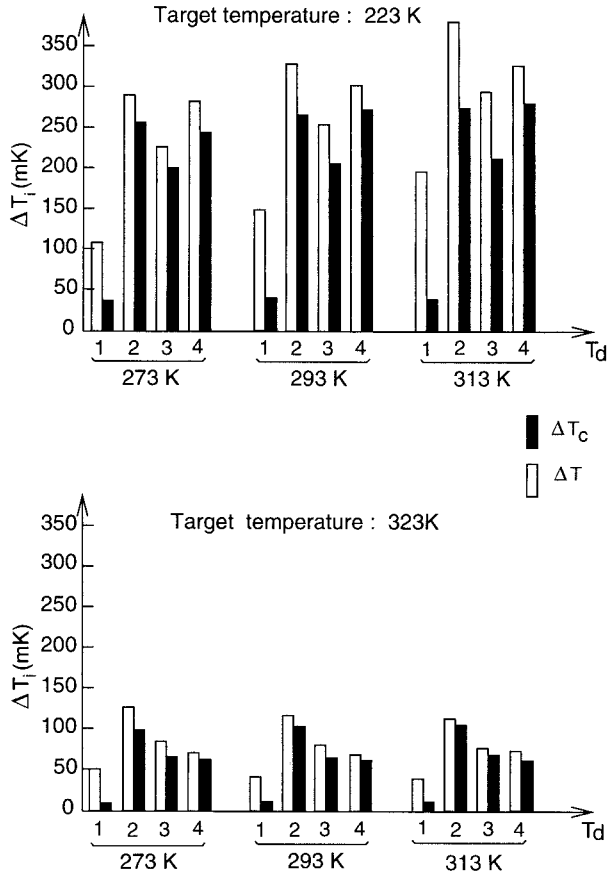

FIG. 10. Global uncertainties (noises + biases) ΔT_i for two retrieved target brightness temperature (223 and 323 K) as a function of the detector temperature T_d for 1-s measurements. We have also reported the uncertainty on the output signal ΔT_i^c. The four channels W, N12, N11, and N9 are labeled as 1, 2, 3, and 4, respectively.

that a calibration be performed, before and after every measurement campaign, especially if a high accuracy is demanded.

e. Impact of a thermal shock

First, it should be recalled that the instrument cavity is not temperature stabilized. This option is suitable for a better in-field autonomy. However, it is necessary to check the behavior of the instrument for a fast change of the cavity temperature, as this is to happen in the field, for sudden changes of the ambient conditions. For this, the instrument was subjected to a thermal shock in the laboratory. The radiometer was set in a thermal cell. A temperature step was programmed in order to quickly increase the temperature of the cell from 293.5 to 305 K. The measured temperature variations of the detector are presented in Fig. 11 as a function of the time. Different conditions are successively met: (i) equilibrium of the cell before the thermal shock applied at 1045 LT, (ii) quick temperature increase in response to the thermal shock from 1045 to 1130 LT, and (iii) slower

TABLE 7. Biases expressed in brightness temperature variations induced by the long-term change of the instrument sensitivities through each channel.

Channel i	ΔT_i^d (K)
W	0.36
N12	0.30
N11	0.30
N9	0.37

temperature variations between 1130 and 2100 LT. The observed heating rate of the detector during the thermal shock is in agreement with the measured thermal inertia of the optical head (corresponding to a time constant of around 45 mn). To test the accuracy of the measurements when the instrument is in a state of strong thermal unbalance, the temperature of a blackbody was derived from the radiometric measurements and compared with its direct measurements by a platinum probe. Figure 12 shows the differences between these determinations for the four channels. Table 8 summarizes the average and the standard deviation of these differences. No significant differences is observed during the thermal shock.

The blackbody temperature is shown to be determined from the radiometric measurements with a bias smaller than 0.15 K in all channels, when compared to the platinum probe measurements. Temperature fluctuations are characterized by a standard deviation smaller than 0.05 K for all channels.

4. Summary and conclusions

The new infrared radiometer CLIMAT, was designed to perform accurate in situ measurements of radiance

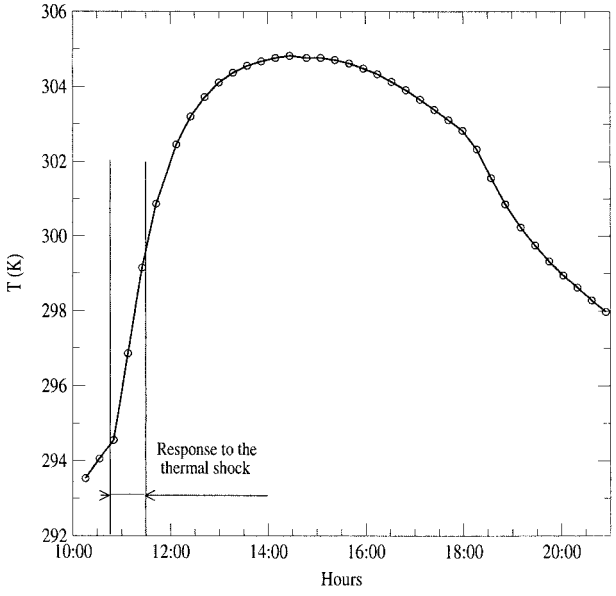

FIG. 11. Variation of the temperature of the detector T_d during a thermal shock.

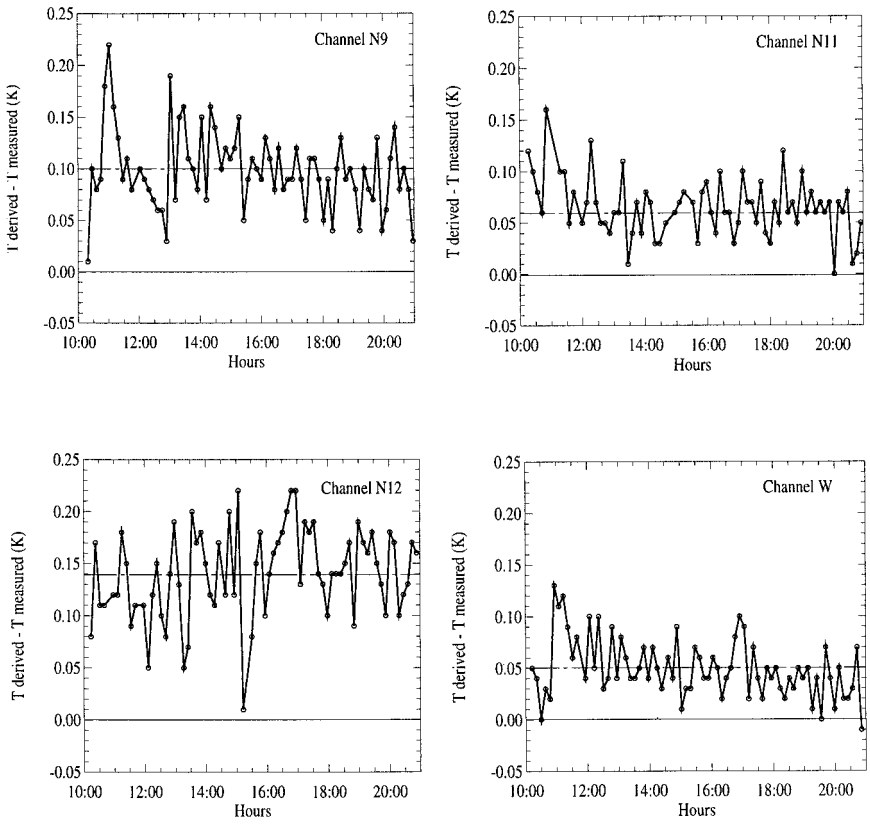

FIG. 12. Differences between the temperature of a blackbody source derived from the radiometric measurements and its direct measurement using a platinum probe, during the thermal shock.

or brightness temperature. It can operate with up to six channels in the spectral domain ranging from 8 to 14 μm. The basic principle of the measurements consists in a comparison between the radiances of the target and that of the detector cavity used as a reference. This cavity is viewed with a retractable mirror moved at will, whenever a reference radiance is considered necessary. The optical performance of the prototype was characterized experimentally showing a sharply delimited field of view at a value of 10°. The asymmetry in the field was explained using a Monte Carlo ray-trace model and attributed to small uncertainties in the assembly process. Due to the optical design, the field of view could easily be modified by changing the objective focal length. Albeit the cavity is not thermostatically controlled, the accuracy of the measurements is not significantly degraded by the application of a thermal shock of 12 K.

TABLE 8. Averaged biases and standard deviations on the radiometric retrieval of a blackbody source temperature compared to its direct measurement during a thermal shock.

Channel *i*	W	N12	N11	N9
Average (K)	0.05	0.14	0.06	0.10
Std dev (K)	0.03	0.04	0.03	0.04

Typically, the radiometric noise expressed as an equivalent change in brightness temperature (NEDT) is in the order of 50 mK for a 1-μm bandwidth at room temperature. The instrument sensitivity showed remarkable stability over the entire test period (seven months). The measurements are usually realized over 1-s periods but can be shortened to 20 ms so as to match requirements for airborne use. Then, the performances of the prototype instrument in our laboratory are deemed to be satisfactory, based on initial requirements. The electrical autonomy, the automated operation, the portability, and the versatility to varied conditions of the instrument, were experimented in situ and proved to be satisfactory, during several field experiments described in the companion paper.

Acknowledgments. This work was supported by the Centre National d'Etudes Spatiales (CNES) under Contract 93/CNES/0373. Thanks are due to J. P. Buis and G. Clave from CIMEL Electronique, who participated very actively to the radiometer manufacturing. The authors are specially grateful to G. Guyot from the Institut National de la Recherche Agronomique who managed the project. We thank F. Herlemont from the Laboratoire de Spectroscopie Hertzienne, B. Sombret from the La-

boratoire de Spectroscopie Infrarouge et Raman, and L. Menenger from the Laboratoire de Météorologie Dynamique for their contributions to the optical studies.

REFERENCES

Abuhassan, N. K., 1995: Développement d'un radiomètre infrarouge multispectral de terrain, et premières applications. Ph.D. thesis, Sciences de la Terre, Université de Paris VI, 147 pp.

Barkstrom, B. R., and G. L. Smith, 1986: The Earth Radiation Budget Experiment: Science and implementation. *Rev. Geophys.,* **24,** 379–390.

Brogniez, G., J. C. Buriez, V. Giraud, F. Parol, and C. Vanbauce, 1995: Determination of effective emittance and a radiatively equivalent microphysical model of cirrus from ground-based and satellite observations during the International Cirrus Experiment: The 18 October 1989 case study. *Mon. Wea. Rev.,* **123,** 1025–1036.

Chédin, A., and N. A. Scott, 1991: Observation spatiale du système terre-océan-atmosphère à haute résolution dans l'infrarouge thermique: Perspectives et problèmes. *Proc. Fifth Coll. Int. Physical Measurements and Signatures in Remote Sensing,* Courchevel, France, CNES, 145–146.

Durpaire, J. P., T. Phulpin, and P. Hollier, 1995: IRSUTE a multispectral IR observation instrument on a small satellite. *Proc. Coll. Int. SPIE,* San Diego, CA, SPIE, 843–852.

Fouquart, Y., B. Bonnel, G. Brogniez, J. C. Buriez, L. Smith, J. J. Morcrette, and A. Cerf, 1987: Observations of Saharian aerosols: Results of ECLATS field experiment. Part II: Broadband radiative characteristics of the aerosols and vertical radiative flux divergence. *J. Climate Appl. Meteor.,* **26,** 38–52.

Haeffelin, M., J. R. Mahan, and K. Priestley, 1997: Predicted dynamic electrothermal performance of thermistor bolometer radiometers for earth radiation budget applications. *Appl. Opt.,* **110,** 7129–7142.

Hepplewhite, C. L., 1989: Remote observation of the sea surface and atmosphere. The oceanic skin effect. *Int. J. Remote Sens.,* **10,** 801–810.

Igarashi, T., 1997: The early results from OCTS on board ADEOS. *Geocarto Int.,* **12,** 27–34.

Jamieson, J. A., R. H. Mc Fee, G. N. Plass, R. H. Grube, and R. G. Richards, 1963. *Infrared Physics and Engineering.* McGraw-Hill, 673 pp.

Kandel, R., and Coauthors, 1998: The ScaRaB earth radiation budget dataset. *Bull. Amer. Meteor. Soc.,* **79,** 765–783.

King, M. D., Y. J. Kaufman, W. P. Menzel, and D. Tanré, 1992: Remote sensing of cloud, aerosol, and water vapor properties from the Moderate Resolution Imaging Spectrometer (MODIS). *IEEE Trans. Geosci. Remote Sens.,* **30,** 2–27.

Lorenz, D., 1968: Temperature measurements of natural surfaces using infrared radiometers. *Appl. Opt.,* **7,** 1705–1710.

Mason, B., and J. Schmetz, 1992: Meteorological satellites. *Int. J. Remote Sens.,* **13,** 1153–1172.

McClatchey, R. A., R. W. Fenn, J. E. A. Selby, F. E. Volz, and J. S. Garing, 1971: Optical properties of the atmosphere (revised). AFCRL-71-0279, Environmental Research Paper 354, 85 pp. [Available from Air Force Geophysical Laboratory, LG Hanscom, FIEL, Hanscom AFB, MA 01731.]

Mutlow, C. T., A. M. Zàvody, I. J. Barton, and D. T. Llewellyn-Jones, 1994: Sea surface temperature measurements by the along-track scanning radiometer on the *ERS-1* satellite: Early results. *J. Geophys. Res.,* **99,** 22 575–22 588.

Phulpin, T., and M. Chevrel, 1994: The French space program for Earth observation: Space missions for biosphere studies. *Proc. Sixth Coll. Int. Physical Measurements and Signatures in Remote Sensing,* Val d'Isère, France, CNES, 1201–1205.

Pietras, C., 1996: Développement d'un radiomètre infrarouge thermique multicanal: Qualification du prototype large champ CLIMAT. Ph.D. thesis, Université des Sciences et Technologies de Lille, 178 pp.

Platt, C. M. R., 1971: A narrow beam radiometer for atmospheric radiation studies. *J. Appl. Meteor.,* **10,** 1307–1313.

Saunders, P. M., 1967: Aerial measurement of sea surface temperature in the infrared. *J. Geophys. Res.,* **72,** 4109–4117.

——, 1970: Corrections for airborne radiation thermometry. *J. Geophys. Res.,* **75,** 7596–7601.

Saunders, R. W., and P. J. Minnett, 1990: The measurement of sea surface temperature from C-130. MRF Internal Note 52, 12 pp. [Available from Meteorological Research Flight, Royal Aerospace Establishment, Farnborough, Hampshire GU14 6TD, United Kingdom.]

Weiss, M., 1971: Airborne measurements of earth surface temperatures (ocean and land) in the 10–12 μm and 8–14 μm regions. *Appl. Opt.,* **10,** 1280–1287.

Wielicki, B. A., B. R. Barkstrom, E. F. Harrison, R. B. Lee III, G. L. Smith, and J. E. Cooper, 1996: Clouds and the Earth's Radiant Energy System (CERES): An earth observing system experiment. *Bull. Amer. Meteor. Soc.,* **77,** 853–868.

Wolfe, W. L., and G. J. Zissis, 1989: *The Infrared Handbook.* IRIA Center Environmental Research Institute of Michigan, 1668 pp.